

Radial Velocities of Galactic O-Type Stars. II. Single-lined Spectroscopic Binaries

S. J. Williams, D. R. Gies

*Center for High Angular Resolution Astronomy and
Department of Physics and Astronomy,
Georgia State University, P. O. Box 4106, Atlanta, GA 30302-4106;
swilliams@chara.gsu.edu, gies@chara.gsu.edu*

T. C. Hillwig¹

*Department of Physics and Astronomy, Valparaiso University, Valparaiso, IN, 46383;
todd.hillwig@valpo.edu*

M. V. McSwain¹

*Department of Physics, Lehigh University, 16 Memorial Drive East, Bethlehem, PA 18015;
mcswain@lehigh.edu*

W. Huang²

*Department of Astronomy, University of Washington, Box 351580, Seattle, WA
98195-1580; hwenjin@astro.washington.edu*

ABSTRACT

We report on new radial velocity measurements of massive stars that are either suspected binaries or lacking prior observations. This is part of a survey to identify and characterize spectroscopic binaries among O-type stars with the goal of comparing the binary fraction of field and runaway stars with those in clusters and associations. We present orbits for HDE 308813, HD 152147, HD 164536, BD−16°4826 and HDE 229232, Galactic O-type stars exhibiting single-lined spectroscopic variation. By fitting model spectra to our observed spectra we

¹Visiting Astronomer, Cerro Tololo Inter-American Observatory, National Optical Astronomy Observatory, which are operated by the Association of Universities for Research in Astronomy, under contract with the National Science Foundation.

²Visiting Astronomer, Kitt Peak National Observatory, National Optical Astronomy Observatory, which is operated by the Association of Universities for Research in Astronomy (AURA) under cooperative agreement with the National Science Foundation.

obtain estimates for effective temperature, surface gravity, and rotational velocity. We compute orbital periods and velocity semiamplitudes for each system and note the lack of photometric variation for any system. These binaries probably appear single-lined because the companions are faint and because their orbital Doppler shifts are small compared to the width of the rotationally broadened lines of the primary.

Subject headings: binaries: spectroscopic – stars: early-type – stars: fundamental parameters

1. Introduction

The multiplicity frequency of O-type stars in clusters or associations is large. Sana et al. (2011) find that $\approx 44\%$ of O-stars in open clusters are members of relatively short period, spectroscopic binaries. Mason et al. (1998, 2009) considered the total numbers of spectroscopic (short period) and angularly resolved binaries (long period) and derived an estimate of $\approx 75\%$ for O-stars with some companion, but this estimate must be a lower limit because the intermediate period range (years to decades) remains largely unexplored. Spectroscopic detection of companions to O stars presents many problems. The high luminosities of early-type stars can easily outshine spectroscopic companions with a difference of just a few temperature subtypes, and/or a single luminosity class. Some O stars are rapid rotators with broad lines that can hide the spectral features of a companion, even with high resolution spectra. Systems may also be seen at an unfavorable inclination to our line of sight, reducing the shifts of spectral features that would be observed. Some combination of these three scenarios results in the detection of such systems as low-amplitude, single-lined spectroscopic binaries (SB1), or no detection of velocity variability at all.

We present results on five such systems here that were observed as part of a larger group of O-type stars with little prior observational work and that appear with a binary designation of “U” (unknown) or “?” (uncertain) in Mason et al. (1998). The current status of each of these systems is either unknown spectroscopic variability (HDE 229232 and BD–16°4826) or known variability but with insufficient data to compute an orbit (HDE 308813, HD152147, and HD 164536). With new data presented here (§2), we measure radial velocities, determine orbital elements, and compute stellar parameters for each system (§3), closely following the procedure used to analyze velocity non-variables in Paper I of this series (Williams et al. 2011). We discuss these first single-lined spectroscopic orbits and physical parameters for each system (§4). We conclude the paper with a discussion about the nature of the unseen companions (§5).

2. Observations

Observations of HDE 308813, HD 152147, BD–16°4826, and HD 164536 were obtained from 2003 March 16 to 20 UT, 2004 January 13 to 29 UT, and May 27 to June 8 UT with the Cerro Tololo Inter-American Observatory (CTIO) 1.5 m telescope and RC spectrograph. We used grating #47 (831 lines per mm, 8000 Å blaze wavelength in the first order Littrow configuration) in second order together with a BG39 or CuSO₄ order blocking filter with a slit width of 2". The detector was a Loral 1200 × 800 CCD. This arrangement produced spectra covering the range 4058 – 4732 Å with a FWHM resolving power of $R = \lambda/\Delta\lambda \approx 2750$ and a wavelength calibration accuracy of $\sim 4 \text{ km s}^{-1}$ based on the rms scatter of fits to comparison spectra. The instrumental broadening from this setup, found from the FWHM of the comparison lines, was computed to be equivalent to a Doppler broadening of 109 km s⁻¹. Exposure times were several minutes in order to reach a signal-to-noise ratio (S/N) exceeding 100 per pixel. Each observation was bracketed with HeAr comparison spectra for wavelength calibration, and numerous bias and flat field spectra were obtained each night.

HDE 229232 was observed with the Kitt Peak National Observatory (KPNO) 2.1 m telescope during an observing run from 2008 November 15 to 21 UT. These observations made use of the Goldcam spectrograph with grating G47 (831 grooves mm⁻¹) in second order with a CuSO₄ order sorting filter. The detector was the T3KC CCD (a 3072 × 1024 pixel array with 15 × 15 μm pixels), and the slit width was set to 1".3 resulting in spectra with a FWHM resolving power of $R = \lambda/\Delta\lambda = 3030$. The exposure time for HDE 229232 was 600 s, enabling a S/N of about 200 per pixel in the continuum. The wavelength range is 3942 – 5032 Å with a wavelength calibration accuracy of $\sim 5 \text{ km s}^{-1}$ based on the rms scatter of fits to comparison lines. Instrumental broadening for these data, again estimated from the FWHM of comparison lines, was found to be 99 km s⁻¹.

All spectra were reduced using standard routines in IRAF³ and then rectified to unit continuum via fitting line-free regions. Next, all spectra for a specific target were transformed to a common heliocentric wavelength grid in log λ increments and were placed into a two dimensional array as a function of spectrum wavelength and time. The subsequent velocity measurements and analysis of spectra may then be done on the entire array of spectra, rather than on each individual spectrum.

³IRAF is distributed by the National Optical Astronomy Observatory, which is operated by the Association of Universities for Research in Astronomy, Inc., under cooperative agreement with the National Science Foundation.

3. Radial Velocities and Stellar Parameters

To measure both velocities and stellar parameters, we began with an approximate model template for the star. A simple “by eye” fit to several prominent absorption features was made by interpolating in the OSTAR2002 grid (Lanz & Hubeny 2003) for stars with $T_{\text{eff}} > 30$ kK and in the BSTAR2006 grid (Lanz & Hubeny 2007) for stars cooler than 30 kK.

Velocities for each spectrum for each object were then measured using the standard method of cross-correlation, and the uncertainty in the resulting velocity was estimated using the method of Zucker (2003). The model was cross-correlated with each spectrum in the particular object’s spectrum stack. Prior to cross-correlation, object dependent emission features and interstellar features were removed, including the broad diffuse interstellar band (DIB) near $\lambda 4428 \text{ \AA}$. The radial velocities are listed in Table 1 with targets ordered by right ascension. The table lists the object name, Heliocentric Julian date of observation, orbital phase (see below), radial velocity, velocity uncertainty, and the observed minus calculated ($O - C$) value for each measurement. Note that the quoted velocity uncertainties do not include those uncertainties related to the wavelength calibration of the spectra.

For each object, we ran fits of the radial velocity measurements for eccentric orbits and for circular orbits using the nonlinear, least-squares fitting routine from Morbey & Brosterhus (1974). We note that we did not use any other period search algorithm because our data sets covered all of or significant fractions of each orbital period, so there was no ambiguity in the selection of an initial period estimate for the general orbital fitting scheme. Following Lucy & Sweeney (1971), we computed a statistic based on the rms of the fit for the eccentric and circular cases, $p = (\text{rms}_e/\text{rms}_c)^\beta$, where rms_e is the rms for the eccentric orbital fit, rms_c that for the circular orbital fit, and $\beta = (N - M)$, where N represents the number of observations, and M the number of parameters fit (6 for the eccentric case). Values of $p > 0.05$ (the 5% significance level) indicate that the eccentric orbit does not statistically improve the fit. For each of the orbits computed here, the eccentric fits provided no significant improvement in the residuals, so we adopted circular orbits. The circular orbital parameters of period, P , the time of maximum velocity, T_0 , the systemic velocity for the system, γ , and the velocity semiamplitude, K_1 , are listed in Table 2. Also listed are the mass function, $f(m)$, the projected orbital semi-major axis, $a_1 \sin i$, the rms of the fit, and the number of observations. The radial velocities and orbital solutions are plotted in Figures 1 through 5, as are the uncertainties associated with the wavelength calibration, σ_λ . Using the final orbit fits we employed a shift-and-add algorithm to the spectrum stack in order to create a higher S/N master spectrum. These spectra are plotted in Figure 6.

Stellar parameters were estimated by fitting the master spectrum for each object with model templates from OSTAR2002 (Lanz & Hubeny 2003) and BSTAR2006 (Lanz & Hubeny

2007). Initial values for $v \sin i$ were estimated by convolving the model template with the instrumental broadening (see §2) and with a projected rotational velocity ($v \sin i$) function to obtain a broadening function making a rough match of one prominent non-hydrogen absorption line. The choice of the absorption line used differed based on the temperature of the star. We adopted linear limb darkening coefficients from Wade & Rucinski (1985). A least squares grid search routine was then employed to refine the estimates of T_{eff} and $\log g$ from fits to several spectral features (listed for each individual object in the following section). These updated estimates for T_{eff} and $\log g$ were then used to refine the $v \sin i$ value by comparison of the FWHM measurements of lines in the master spectrum with those from the model template broadened for a range of $v \sin i$. The adopted T_{eff} and $v \sin i$ values are means of individual line measurements with uncertainties computed from the standard deviation of the measurements of different lines. For $\log g$, we used a weighted average where Balmer line wing fits are given twice as much weight in the calculation of means because of their sensitivity to pressure broadening. It should be noted that we cannot measure $v \sin i$ values less than roughly half our instrumental broadening, or about 50 km s^{-1} . Another limitation is that both OSTAR2002 (Lanz & Hubeny 2003) and BSTAR2006 (Lanz & Hubeny 2007) are based on plane-parallel approximations and solar helium abundances. These approximations may be less accurate for very high luminosity stars, such as HD 152147, which generally have extended atmospheres and significant winds. Lower values for $\log g$ indicate the star is evolved, and such stars may also have enhanced helium abundances due to mixing and mass loss. The entire process of fitting stellar parameters was repeated once to ensure accuracy of the final results.

The derived T_{eff} , $\log g$, and $v \sin i$ values are listed in Table 3, along with a spectral classification estimate made by comparing our computed values for T_{eff} and $\log g$ with Tables 4, 5, and 6 of Martins et al. (2005) for O-stars, and Table 2 from Böhm-Vitense (1981) for the two targets on the border between O- and B-type stars, HDE 308813 and HD 152147. Column 2 in the table lists the spectral classifications for the primary component found in the literature. The final three columns in Table 3 list the parameters used to obtain a spectroscopic parallax distance estimate that is described in detail for each object in the next section.

4. Discussion of Individual Objects

4.1. HDE 308813

The variable velocity of HDE 308813 and its membership in cluster IC 2944 were first suggested by Thackeray & Wesselink (1965) based on three observations spaced two years

apart. They suggested that HDE 308813 may be an SB2 due to differences in velocities from He II compared to other lines seen on their last plate. Huang & Gies (2006) also measured three velocities, over a time span of 4 days, and suggested the system was a possible single-lined spectroscopic binary. Sana et al. (2011) gathered 11 velocities over time spans of days to years, and they were therefore unable to discern an orbital period or ephemeris for this system, although they did confirm the SB1 nature suggested by Huang & Gies (2006). The observations reported here have the benefit of being made over three separate epochs, the second one a 16 day span. Our computed orbital period of 6.340 d (Table 2) is therefore covered twice in that time span. The radial velocity measurements from Thackeray & Wesselink (1965) (-12 , 18 , and -40 km s $^{-1}$), Ardeberg & Maurice (1977) (-10 km s $^{-1}$), and Huang & Gies (2006) (21.9 , -13.4 , and -17.6 km s $^{-1}$) all span the range of velocities we observe. The data from Huang & Gies (2006) are overplotted in Figure 1, but were not used in computation of the orbit. Including any of the archival data increased the rms of the fit by at least a factor of two (presumably due to differences in the way the velocity was measured by these authors), so we only fit data reported in this work.

Prior $v \sin i$ measurements are 186 ± 11 km s $^{-1}$ by Daffon et al. (2007) (using He I $\lambda\lambda 4026, 4387, 4471$), 196 ± 9 km s $^{-1}$ by Huang & Gies (2006) (who used the same lines plus Mg II $\lambda 4481$), and 197 km s $^{-1}$ by Penny et al. (2004) (from UV lines in spectra obtained by the Hubble Space Telescope and Space Telescope Imaging Spectrograph). All of these measurements agree within 1σ of our computed value of 204 ± 10 km s $^{-1}$ obtained by measuring He I $\lambda\lambda 4143, 4387, 4471$. T_{eff} and $\log g$ were estimated using H δ , H γ , He I $\lambda\lambda 4143, 4387$, and He II $\lambda 4686$. Based on the values computed above and the calibration of Böhm-Vitense (1981), the spectral classification of HDE 308813 is B0 V. This is very close to the classification by Schild (1970) of O9.5 V.

We can estimate the distance to HDE 308813 via spectroscopic parallax. Thackeray & Wesselink (1965) measured $V = 9.28$ and $(B - V) = 0.04$ for HDE 308813. We adopt $(B - V)_0 = -0.26$ for a B0 V star from Wegner (1994) and $M_V = -3.90$ for an O9.5 V star from Martins et al. (2005). Assuming $R_V = 3.1$ leads to a distance of 2.82 kpc, and this value is listed in Column 9 of Table 3. This distance puts HDE 308813 a bit further than the distance for IC 2944 of 2.2 kpc from Tovmassian et al. (1998), but it may be a member of a more distant association (see their Table 5). It should also be noted that the difference in the distances may be due to the uncertainties in our estimation of $(B - V)$, $(B - V)_0$, M_V , and R_V . However, Dias et al. (2002) report an average cluster velocity for IC 2944 of -4.8 ± 5.1 km s $^{-1}$. The systemic velocity from our orbital fit for HDE 308813 is 8.5 km s $^{-1}$, 2.6σ from the cluster average, making cluster membership unlikely.

4.2. HD 152147

HD 152147 lies in the vicinity of the Galactic open cluster NGC 6231, but it is not likely to be a member. A number of velocities have been previously published, five by Struve (1944), one by Conti et al. (1977), and 10 by Levato et al. (1988), who were also the first to claim velocity variability. We fit an orbit to all these literature velocities and our own 15 measurements with equal weight and obtain the parameters listed in Table 2 with the orbit shown in Figure 2.

Conti & Ebbets (1977) measured $v \sin i = 80 \text{ km s}^{-1}$ by comparing $\text{H}\gamma$, He I $\lambda\lambda 4387, 4471$, and He II $\lambda 4541$ with calibrated standard stars. We measure a rotational velocity of $150 \pm 28 \text{ km s}^{-1}$ from fits to Si IV $\lambda 4088$, He I $\lambda\lambda 4143, 4471, 4387$, and He II $\lambda 4686$. Their spectra were obtained at higher resolution than our spectra, so our measurement should be taken as an upper limit. The estimates for T_{eff} and $\log g$ were made from fits to $\text{H}\gamma$, He I $\lambda\lambda 4143, 4387$, and He II $\lambda 4686$. Using these numbers in concert with the calibration in Martins et al. (2005), we estimate the spectral classification for HD 152147 to be O9.5 I, very close to the spectral classification given by Walborn (1972), O9.7 Ib.

To estimate the spectroscopic parallax, we began with $V = 7.23$ and $(B - V) = 0.37$ measured by Schild et al. (1969) from seven observations. Wegner (1994) gives a value of $(B - V)_0 = -0.24$ for an O9.5 I star. Further assuming a standard value of $R_V = 3.1$ and using $M_V = -6.28$ in Martins et al. (2005) for an O9.5 I star, leads to a calculated distance to HD 152147 of 2.11 kpc. This value does not agree well with the recent distance estimate for HD 152147 of $1.64 \pm 0.24 \text{ kpc}$ from Megier et al. (2009) that is based on interstellar line strength. Nor does this value match with the distance estimate to NGC 6231 given by Sana et al. (2006) of 1.64 kpc. This may mean our estimate for R_V is inaccurate for the line of sight to HD 152147, but this also may be evidence suggesting that HD 152147 is not a member of NGC 6231. For example, Humphreys (1978) places this star in the Sco OB1 association at a distance of 1.91 kpc, a distance closer to our estimate. Furthermore, Kharchenko et al. (2005) reports that NGC 6231 has an average cluster radial velocity of $-27.28 \pm 2.98 \text{ km s}^{-1}$, far different than our systemic velocity from the orbital fit of $-40.1 \pm 0.7 \text{ km s}^{-1}$.

4.3. HD 164536

The first radial velocity measurement published is by Hayford (1932) who reports a value of 6 km s^{-1} from five spectral lines in a single spectrum. Other radial velocities are averages from several, typically unspecified, nights: $-11.1 \pm 3.2 \text{ km s}^{-1}$ from five plates

reported by Neubauer (1943) and -10 km s^{-1} from three plates reported by Feast et al. (1955). None of these velocities were used in the derivation of the orbital parameters listed in Table 2.

HD 164536 is one of the brightest members of the cluster NGC 6530 (Walker 1957; Boggs & Böhm-Vitense 1989). A proper motion study was made of NGC 6530 by van Altena & Jones (1972), who claim that HD 164536 is not a member. However, its cluster membership was reestablished in a series of papers based on *IUE* spectra (Böhm-Vitense et al. 1984; Boggs & Böhm-Vitense 1989, 1990). Africano et al. (1975) claimed detection of a nearby companion during a lunar occultation observation at $\rho = 0''.174 \pm 0''.003$ arcsec, $\theta = 203^\circ$, and $\Delta m = 2.2 \pm 0.4$ mag. Subsequent follow up observations that had the ability to see such a companion (Mason 1996; Turner et al. 2008) did not resolve this close companion. This star is the brightest of a trapezium (4 star) system listed in the Washington Double Star Catalog (WDS; Mason et al. 2001). Turner et al. (2008) resolve the closest component at $1''.7$ distant, with other members outside of their field of view. This close component is too faint ($V = 12.4$ according to the WDS) compared to HD 164536 ($V = 7.1$; Høg et al. 2000) to influence our spectra.

To derive the effective temperature and $\log g$, $\text{H}\delta$, $\text{H}\gamma$, $\text{He I } \lambda 4471$, and $\text{He II } \lambda \lambda 4541, 4686$ were used. The projected rotational velocity was computed from observations of the He II lines. Boggs & Böhm-Vitense (1989) arrive at an effective temperature of 32 kK determined from optical photometry and spectral type of O9 V from their analysis of *IUE* spectra. The value derived here of 37.4 ± 0.9 kK is $> 3\sigma$ higher, indicating an O6.5 V estimate of the spectral classification from Table 4 in Martins et al. (2005). This classification is also at odds with the optical classification reported by MacConnell & Bidelman (1976) of O9 III, although the spectrum is noted as being overlapped with another star, making the classification uncertain. Houk & Smith-Moore (1988) find a spectral type of O7/O8, closer to our estimate. Given the uncertainties in the spectral classifications in MacConnell & Bidelman (1976) and Boggs & Böhm-Vitense (1989), we think our estimate of O6.5 V matches well with that of Houk & Smith-Moore (1988), and is currently the best estimate.

We estimate the distance to HD 164536 by taking the Tycho B and V magnitudes (Høg et al. 2000) transformed to Johnson magnitudes, an $M_V = -4.77$ for an O6.5 V (Martins et al. 2005), $(B - V)_0 = -0.29$ (Wegner 1994), and assume $R_V = 3.1$. This results in a distance of 1.78 kpc, equal to the 1.78 kpc estimate given by van Altena & Jones (1972) and larger than the 1.33 kpc distance from Kharchenko et al. (2005). Using $R_V = 3.45$ for HD 164536, as reported in Wegner (2003), the distance drops to 1.71 kpc. Both of the distances computed in this work agree within uncertainties with the distance reported by van den Ancker et al. (1997) of 1.8 ± 0.2 kpc. The systemic velocity component of HD 164536

found here is -4.9 ± 1.1 km s $^{-1}$; this value is 1.3σ from the cluster radial velocity of NGC 6530 listed by Barbier-Brossat & Figon (2000) of -13.32 ± 6.34 km s $^{-1}$. This appears to offer tentative support for the inclusion of HD 164536 in NGC 6530.

4.4. BD–16° 4826

No earlier velocity measurements were found in the literature for BD–16°4826, making our 11 velocities and SB1 fit the first published. However, additional observations are desirable because our observing span of 12 d is somewhat smaller than the 16 d orbital period. Consequently, the orbital parameters should be considered as preliminary values.

BD–16°4826 is a member of the cluster NGC 6618 which is embedded in M 17. Estimates for effective temperature and $\log g$ were made from fits to H δ , H γ , He II $\lambda\lambda$ 4200, 4541, 4686 and He I $\lambda\lambda$ 4387, 4471. We used He II $\lambda\lambda$ 4541, 4686 to derive the $v \sin i$ value listed in Table 3. There was very large scatter in our attempts to fit the spectrum of BD–16°4826, as evidenced by the highest uncertainties for stellar parameters in this work. Listed as an O5 in Hiltner & Johnson (1956), the spectral classification of this object has varied from O3 V based on optical spectra (Garmany & Vacca 1991) to any of four spectral types ranging from O5 V to O9 III that were based upon IR data by Povich et al. (2009). The best estimators we have available as luminosity criteria are the wings of the Balmer lines. These definitively rule out the possibility of BD–16°4826 being evolved (see Fig. 6 and Table 3), and we estimate the spectral classification for BD–16°4826 to be O5.5 V.

The most recent optical photometry is reported by Ogura & Ishida (1976). They find, from two observations, $V = 9.85$ and $(B - V) = 0.94$. Using $M_V = -5.07$ (Martins et al. 2005), $(B - V)_0 = -0.30$ (Wegner 1994), and a standard value $R_V = 3.1$, we arrive at a spectroscopic distance to BD–16°4826 of 1.60 kpc. The distance to NGC 6618 and M 17 is a topic of some debate. The recent IR study by Povich et al. (2009) lists two distances, 1.6 ± 0.3 kpc from Nielbock et al. (2001) and 2.1 ± 0.2 kpc from Hoffmeister et al. (2008). The value derived here agrees with the Nielbock et al. (2001) estimate. Our computed value is also within the uncertainty of the lower limit on the distance reported by Hanson et al. (1997) of $1.3_{-0.2}^{+0.4}$ kpc based on extinction corrected IR magnitudes of O-stars. The systemic velocity found here for BD–16°4826 of 11.0 ± 1.0 km s $^{-1}$ is 2.2σ different than the cluster velocity of -17 ± 13 km s $^{-1}$ (Kharchenko et al. 2005). This discrepancy in velocities hints that it is less likely that BD–16°4826 is actually a member of NGC 6618.

4.5. HDE 229232

There is very little in the literature about HDE 229232. Like with BD–16°4826, our seven velocities are the first published. However, with only seven data points, our orbit should be considered preliminary. For example, it is possible that the system has a significant eccentricity and longer period, so that our data record the variations around a single periastron point. Our estimate that the star is an O5 V with a variable velocity indicates that this is a massive binary that deserves additional observational work.

To estimate effective temperature and $\log g$, we used the H δ wings, He I λ 4026, and He II λ λ 4200, 4541. Only the helium lines were used to compute the $v \sin i$. Our estimated spectral classification of O5 V is very close to that listed by Walborn (1973) of O4 Vn((f)).

Using $V = 9.525$ and $(B - V) = 0.82$ from Hiltner & Johnson (1956), $M_V = -5.21$ from Martins et al. (2005) and $(B - V)_o = -0.30$ (Wegner 1994) (both values for an O5 V star), and the standard $R_V = 3.1$, the distance to HDE 229232 is 1.79 kpc. The galactic coordinates of HDE 229232 are $\ell = 77^\circ.40$ and $b = 0^\circ.93$, looking down the Cygnus arm, where many associations with a range in distances from 0.75 to 2.32 kpc appear more or less in the same part of the sky (Uyaniker et al. 2001, and references therein). It lies in the direction of the Cyg OB8 association that Humphreys (1978) places at a distance of 2.29 kpc. The systemic velocity from the orbital fit of HDE 229232 is -46.6 ± 0.8 km s $^{-1}$. Mel’Nik & Dambis (2009) report a velocity for Cyg OB8 from velocities in the work of Barbier-Brossat & Figon (2000) of -21 ± 11 km s $^{-1}$. This puts our estimate of the systemic velocity 2.3σ from the mean value for Cyg OB8, perhaps lending support that HDE 229232 is not a member of the Cyg OB8 association, but possibly a member of one of the other associations in that direction.

5. Discussion

The five systems studied here are all relatively long period, low semiamplitude SB1s. The velocity semiamplitudes of these systems range from 13.1 km s $^{-1}$ to 26.2 km s $^{-1}$ with orbital periods ranging from 6.2 to 15.8 days. None of these systems show eclipses or photometric variation in either the All Sky Automated Survey (Pojmański 2002) nor The Amateur Sky Survey (TASS⁴; Droege et al. 2006). The only object with published time series photometry is HD 152147, and Sterken et al. (1993) found no variability. BD–16°4826 is an X-ray source but with a flux typical of single O-stars (Nazé 2009).

⁴<http://sallman.tass-survey.org/servlet/markiv/>

For circular orbits, the orbital semiamplitude is given by

$$K_1 = 289 \text{ km s}^{-1} (M_1/25M_\odot)^{1/3} (P/10 \text{ d})^{-1/3} \frac{q}{(1+q)^{2/3}} \sin i$$

where the mass ratio is $q = M_2/M_1$. Therefore the low K_1 systems in our sample are drawn from those with low mass companions (small q) and/or low inclination. We can estimate the most probable q from the statistical method of Mazeh & Goldberg (1992). This method requires assumptions about the mass ratio distribution of the sample and the mass of the primary, which we estimate from Martins et al. (2005). Based on observations of O-stars (Mason et al. 1998), we assume the mass ratio distribution is uniform. The resultant mass ratios (q) from this distribution are listed in Table 4. Estimates for the spectral classification of the secondary are made by comparing the mass in column 5 to the values listed in Table B.1 of Gray (2005). We assume these companions are all main sequence stars, because all the primary stars are so young. Column 7 lists the difference in V magnitude between the primary and secondary, again as estimated from Gray (2005). These are all greater than 2.3 mag, and they lead to the monochromatic flux ratios given in column 8. The extremely small flux ratios may be part of the reason why companions are not seen in the data.

The true nature of the mass ratio distribution for O-type stars is unknown. (For a discussion of the current state of our understanding of the mass ratio distribution, see the recent work by Kiminki & Kobulnicky (2012).) To explore the range of possibilities besides the flat distribution used above, we take two extreme values for a power law distribution $N(q) = N_0 q^\alpha$. The first is the standard Salpeter distribution (Salpeter 1955) with an exponent of $\alpha = -1.35$. The second has an exponent of $\alpha = 1.0$, a distribution that is more biased toward near equal-mass binaries, as was suggested in Pinsonneault & Stanek (2006). With these mass ratio distributions, and estimates for the masses of the primary and secondary, we can solve for the probable inclination of the orbit based on the mass function. The resulting ranges of mass ratio and inclination are listed in Table 5. These ranges are not large, and the estimates for orbital inclination are low ($i < 37^\circ$).

Taking our values for i and orbital period, combined with an estimate of the stellar radius (Martins et al. 2005), we compute the synchronous rotational velocity, $v \sin i$ (sync), listed in column 10 of Table 4. These numbers are all much smaller than the $v \sin i$ measurements listed in column 5 of Table 3, which is consistent with the idea that these systems are too young to have attained synchronous rotation.

Do the line blending effects of the companions influence our results for $v \sin i$ or K_1 ? To check the magnitude of the effect, we can consider the maximum separation of the spectral features of the individual components. The ratio of maximum Doppler separation to

projected rotational velocity is

$$\frac{K_1(1 + 1/q)}{v \sin i}.$$

By using the mass ratio as computed above, we calculate this separation and list it in column 9 of Table 4. These values are all well below unity, meaning the lines of the components are always blended with those of the primary (except in cases where a lower ionization line appears in the secondary but not in the primary spectrum). The additional fact that the companions are extremely faint means that line blending problems related to measurements of $v \sin i$ and K_1 will be minimal. As an example, we introduced a model spectrum corresponding to a B3 V star, as estimated for the companion to BD–16°4826 (Column 6, Table 4), at a shift of $K_1(1 + 1/q)$ and normalized according to the flux ratio. This object was chosen because it has the largest ratio of $K_1(1 + 1/q)/v \sin i$, so it should show the largest affect of blending problems. We chose a $v \sin i$ of the companion of 20 km s^{-1} . Such very narrow lines would have more influence on the measured parameters of the primary than wider shallower lines. Measuring the velocity in the same way as described above, we compute a maximum offset of 3.6 km s^{-1} for velocity measurements, comparable to the measurement uncertainties on an individual spectrum. We similarly added a secondary model spectrum at $\pm K_1(1 + 1/q)$ to each of the lines used to measure $v \sin i$, and calculated a value 5.0 km s^{-1} higher than previously. Therefore, even for the narrowest lined star in our sample, the uncertainty in $v \sin i$ introduced by the companion is on the order of 5 km s^{-1} . Although the effects are small, the influence of a companion spectrum on the velocity measurements will be to pull the measurement back toward the rest wavelength of the line. This will make K_1 lower, the mass function lower, and thus the estimate of mass ratio and orbital inclination lower. Consequently, the values of q and i in Table 5 are therefore probably lower than the true values.

Companions will also have an influence on T_{eff} and $\log g$ estimates. In the spectral range covered by our data, an O-star has several He II lines that a mid B-star does not. Therefore, the effect will be to make the O-star lines appear shallower, making the O-star appear cooler. He I lines are stronger in B-stars, and in combination with an O-star spectrum will make these lines appear deeper, again causing the O-star spectrum to appear cooler. Thus, our estimates for T_{eff} and $\log g$ are also lower limits and are likely more indicative of the combined spectrum of the binary.

Our results from this analysis suggest that all the objects in this sample are SB1. This is due to three main effects: low orbital inclination, broad spectral features of the primary stars, and faint companions. In the future, high resolution and high S/N spectra may be able to extract the companion spectrum in systems like those studied here (Gies et al. 1994). The next paper in this series will describe double-lined spectroscopic orbits for Galactic O-type

stars where companion spectra are clearly seen.

We are grateful to the directors and staffs of KPNO and CTIO for their help in obtaining these observations. This material is based upon work supported by the National Science Foundation under Grant No. AST-0606861 and AST-1009080. This research has made use of the Washington Double Star Catalog maintained at the U.S. Naval Observatory.

Facility: CTIO:1.5m *Facility:* KPNO:2.1m

REFERENCES

- Ardeberg, A., & Maurice, E. 1977, A&AS, 28, 153
- Africano, J. L., Cobb, C. L., Dunham, D. W., et al. 1975, AJ, 80, 689
- Barbier-Brossat, M., & Figon, P. 2000, A&AS, 142, 217
- Boggs, D., & Böhm-Vitense, E. 1989, ApJ, 339, 209
- Boggs, D., & Böhm-Vitense, E. 1990, ApJ, 358, 441
- Böhm-Vitense, E. 1981, ARA&A, 19, 295
- Böhm-Vitense, E., Hodge, P., & Boggs, D. 1984, ApJ, 287, 825
- Conti, P. S., & Ebbets, D. 1977, ApJ, 213, 438
- Conti, P. S., Leep, E. M., & Lorre, J. J. 1977, ApJ, 214, 759
- Dafon, S., Cunha, K., de Araújo, F. X., Wolff, S., & Przybilla, N. 2007, AJ, 134, 1570
- Dias, W. S., Alessi, B. S., Moitinho, A., & Lépine, J. R. D. 2002, A&A, 389, 871
- Droege, T. F., Richmond, M. W., & Sallman, M. 2006, PASP, 118, 1666
- Feast, M. W., Thackeray, A. D., & Wesselink, A. J. 1955, MmRAS, 67, 51
- Garmany, C. D., & Vacca, W. D. 1991, PASP, 103, 347
- Gies, D. R., Fullerton, A. W., Bolton, C. T., et al. 1994, ApJ, 422, 823
- Gray, D. F. 2005, The Observation and Analysis of Stellar Photospheres, 3rd Edition (Cambridge, UK: Cambridge University Press)

- Hanson, M. M., Howarth, I. D., & Conti, P. S. 1997, *ApJ*, 489, 698
- Hayford, P. 1932, *Lick Obs. Bull.*, 16, 53
- Hiltner, W. A., & Johnson, H. L. 1956, *ApJ*, 124, 367
- Hoffmeister, V. H., Chini, R., Scheyda, C. M., et al. 2008, *ApJ*, 686, 310
- Høg, E., Fabricius, C., Makarov, V. V., et al. 2000, *A&A*, 355, L27
- Houk, N., & Smith-Moore, M. 1988, *Michigan Catalogue of Two-dimensional Spectral Types for the HD Stars, Vol. 4* (Ann Arbor: Univ. of Michigan)
- Huang, W., & Gies, D. R. 2006, *ApJ*, 648, 580
- Humphreys, R. M. 1978, *ApJS*, 38, 309
- Kharchenko, N. V., Piskunov, A. E., Röser, S., Schilbach, E., & Scholz, R.-D. 2005, *A&A*, 438, 1163
- Kiminki, D. C., Kobulnicky, H. A., 2012, *ApJ*, 751, 4
- Lanz, T., & Hubeny, I. 2003, *ApJS*, 146, 417
- Lanz, T., & Hubeny, I. 2007, *ApJS*, 169, 83
- Levato, H., Morrell, N., Garcia, B., & Malaroda, S. 1988, *ApJS*, 68, 319
- Lucy, L. B., & Sweeney, M. A. 1971, *AJ*, 76, 544
- MacConnell, D. J., & Bidelman, W. P. 1976, *AJ*, 81, 225
- Martins, F., Schaerer, D., & Hillier, D. J. 2005, *A&A*, 436, 1049
- Mason, B. D. 1996, *AJ*, 112, 2260
- Mason, B. D., Gies, D. R., Hartkopf, et al. 1998, *AJ*, 115, 821
- Mason, B. D., Hartkopf, W. I., Gies, D. R., Henry, T. J., & Helsel, J. W. 2009, *AJ*, 137, 3358
- Mason, B. D., Wycoff, G. L., Hartkopf, W. I., Douglass, G. G., & Worley, C. E. 2001, *AJ*, 122, 3466
- Mazeh, T., & Goldberg, D. 1992, *ApJ*, 394, 592

- Megier, A., Strobel, A., Galazutdinov, G. A., & Krelowski, J. 2009, *A&A*, 507, 833
- Mel’Nik, A. M., & Dambis, A. K. 2009, *MNRAS*, 400, 518
- Morbey, C. L., & Brosterhus, E. B. 1974, *PASP*, 86, 455
- Nazé, Y. 2009, *A&A*, 506, 1055
- Neubauer, F. J. 1943, *ApJ*, 97, 300
- Nielbock, M., Chini, R., Jütte, M., & Manthey, E. 2001, *A&A*, 377, 273
- Ogura, K., & Ishida, K. 1976, *PASJ*, 28, 35
- Penny, L. R., Sprague, A. J., Seago, G., & Gies, D. R. 2004, *ApJ*, 617, 1316
- Pinsonneault, M. H., & Stanek, K. Z. 2006, *ApJ*, 639, L67
- Pojmański, G. 2002, *Acta Astron*, 52, 397
- Povich, M. S., Churchwell, E., Biegging, J. H., et al. 2009, *ApJ*, 696, 1278
- Salpeter, E. E. 1955, *ApJ*, 121, 161
- Sana, H., Gosset, E., Rauw, G., Sung, H., & Vreux, J.-M. 2006, *A&A*, 454, 1047
- Sana, H., James, G., & Gosset, E. 2011, *MNRAS*, 416, 817
- Schild, R. E. 1970, *ApJ*, 161, 855
- Schild, R. E., Hiltner, W. A., & Sanduleak, N. 1969, *ApJ*, 156, 609
- Sterken, C., Manfroid, J., Anton, K., et al. 1993, *A&AS*, 102, 79
- Struve, O. 1944, *ApJ*, 100, 189
- Thackeray, A. D., & Wesselink, A. J. 1965, *MNRAS*, 131, 121
- Tovmassian, H. M., Epremian, R. A., Hovhannessian, K., et al. 1998, *AJ*, 115, 1083
- Turner, N. H., ten Brummelaar, T. A., Roberts, L. C., et al. 2008, *AJ*, 136, 554
- Uyaniker, B., Fürst, E., Reich, W., Aschenbach, B., & Wielebinski, R. 2001, *A&A*, 371, 675
- van Altena, W. F., & Jones, B. F. 1972, *A&A*, 20, 425
- van den Ancker, M. E., The, P. S., Feinstein, A., et al. 1997, *A&AS*, 123, 63

- Wade, R. A., & Rucinski, S. M. 1985, *A&AS*, 60, 471
- Walborn, N. R. 1972, *AJ*, 77, 312
- Walborn, N. R. 1973, *AJ*, 78, 1067
- Walker, M. F. 1957, *ApJ*, 125, 636
- Wegner, W. 1994, *MNRAS*, 270, 229
- Wegner, W. 2003, *AN*, 324, 219
- Williams, S. J., Gies, D. R., Hillwig, T. C., McSwain, M. V., & Huang, W. 2011, *AJ*, 142, 146
- Zucker, S. 2003, *MNRAS*, 342, 1291

Table 1. Radial Velocity Measurements

Star Name	Date (HJD – 2,450,000)	Orbital Phase	V_r (km s ⁻¹)	σ (km s ⁻¹)	$O - C$ (km s ⁻¹)
HDE 308813	2714.805	0.699	-0.6	1.7	-2.2
HDE 308813	2715.708	0.841	20.6	1.7	4.6
HDE 308813	2715.840	0.862	31.2	1.8	8.2
HDE 308813	2716.707	0.999	27.3	1.7	-3.3
HDE 308813	2716.866	0.024	20.7	1.9	-9.7
HDE 308813	2717.697	0.155	32.8	1.9	12.0
HDE 308813	2717.801	0.171	16.3	1.8	-2.6
HDE 308813	2718.699	0.313	4.5	1.8	4.7
HDE 308813	3017.743	0.484	-13.6	2.0	0.0
HDE 308813	3018.753	0.644	-1.6	1.8	3.6
HDE 308813	3019.735	0.799	16.2	2.0	1.0
HDE 308813	3019.836	0.815	26.0	1.9	8.8
HDE 308813	3020.718	0.954	23.6	1.9	-6.1
HDE 308813	3021.713	0.111	28.1	1.9	2.6
HDE 308813	3021.816	0.127	29.6	1.9	5.7
HDE 308813	3022.721	0.270	-3.7	1.9	-9.5
HDE 308813	3022.865	0.292	-4.7	1.9	-7.4
HDE 308813	3023.702	0.424	-18.5	2.0	-7.3
HDE 308813	3023.806	0.441	-11.2	1.9	0.9
HDE 308813	3027.727	0.059	24.9	2.0	-4.2
HDE 308813	3028.704	0.213	16.4	2.0	3.0
HDE 308813	3028.787	0.227	19.6	2.0	7.8
HDE 308813	3029.744	0.377	-3.8	2.0	3.7
HDE 308813	3030.694	0.527	-11.2	1.9	2.1
HDE 308813	3030.776	0.540	-7.9	2.0	5.1
HDE 308813	3031.712	0.688	-1.4	1.9	-1.5
HDE 308813	3032.636	0.834	10.0	1.9	-9.6
HDE 308813	3032.782	0.857	24.5	2.0	2.2
HDE 308813	3033.713	0.004	34.9	1.9	4.3
HDE 308813	3159.469	0.840	15.0	1.8	-5.4
HDE 308813	3160.463	0.997	26.8	1.8	-3.8
HDE 308813	3162.531	0.323	-1.9	1.8	-0.5
HDE 308813	3163.532	0.481	-20.8	1.9	-7.3
HD 152147	3152.593	0.668	-46.7	2.6	-0.2
HD 152147	3153.620	0.742	-33.6	2.5	7.2
HD 152147	3154.580	0.811	-43.7	2.5	-8.6
HD 152147	3154.811	0.828	-35.1	2.5	-1.2
HD 152147	3155.743	0.896	-32.0	2.7	-2.3
HD 152147	3156.775	0.970	-23.8	3.0	3.5
HD 152147	3157.764	0.042	-26.7	2.5	0.7
HD 152147	3157.874	0.050	-40.4	3.4	-12.7
HD 152147	3158.696	0.109	-29.2	2.5	0.8
HD 152147	3159.714	0.183	-35.0	2.4	-0.2
HD 152147	3160.721	0.256	-41.6	2.5	-1.0
HD 152147	3161.737	0.329	-39.2	2.5	7.1

Table 1—Continued

Star Name	Date (HJD – 2,450,000)	Orbital Phase	V_r (km s ⁻¹)	σ (km s ⁻¹)	$O - C$ (km s ⁻¹)
HD 152147	3162.688	0.398	-60.2	2.6	-9.5
HD 152147	3163.709	0.472	-50.8	2.6	2.2
HD 152147	3164.599	0.536	-57.7	2.7	-4.8
HD 164536	3152.753	0.559	-26.6	2.0	2.7
HD 164536	3153.777	0.636	-27.4	1.9	-5.3
HD 164536	3153.916	0.646	-17.0	1.9	3.7
HD 164536	3154.781	0.711	-7.5	1.8	3.8
HD 164536	3155.720	0.782	2.1	1.9	1.9
HD 164536	3156.633	0.850	14.4	2.0	3.9
HD 164536	3156.910	0.871	4.8	2.0	-8.3
HD 164536	3157.881	0.943	15.1	2.0	-4.5
HD 164536	3158.803	0.012	20.4	1.9	-0.7
HD 164536	3159.750	0.083	21.0	1.9	3.2
HD 164536	3160.773	0.160	19.0	1.9	9.9
HD 164536	3161.842	0.240	-4.9	2.1	-1.5
HD 164536	3162.789	0.311	-26.5	2.0	-11.8
HD 164536	3163.779	0.385	-19.5	1.9	5.0
HD 164536	3164.751	0.458	-31.3	2.0	-1.1
HD 164536	3164.870	0.467	-30.8	2.0	-0.3
BD-16°4826	3152.899	0.391	-0.7	2.5	-0.5
BD-16°4826	3153.797	0.445	2.9	2.3	5.4
BD-16°4826	3153.929	0.453	1.6	2.5	4.3
BD-16°4826	3154.913	0.513	-6.1	2.3	-2.8
BD-16°4826	3156.646	0.617	3.9	2.4	3.5
BD-16°4826	3157.914	0.693	5.2	2.4	-0.7
BD-16°4826	3158.901	0.753	13.8	2.3	2.6
BD-16°4826	3159.902	0.813	13.4	2.5	-2.9
BD-16°4826	3161.900	0.934	26.6	2.7	2.9
BD-16°4826	3162.901	0.994	22.3	2.4	-2.6
BD-16°4826	3164.888	0.114	20.2	2.4	-1.2
HDE 229232	4785.649	0.198	-37.5	2.5	4.0
HDE 229232	4786.594	0.351	-56.1	2.2	-0.2
HDE 229232	4787.576	0.511	-69.7	2.1	-7.5
HDE 229232	4788.576	0.673	-47.4	2.2	6.5
HDE 229232	4789.583	0.836	-37.1	2.1	1.4
HDE 229232	4790.572	0.997	-37.5	2.1	-6.5
HDE 229232	4791.574	0.160	-36.9	2.1	1.3

Table 2. Circular Orbital Elements

Parameter	HDE 308813	HD 152147	HD 164536	BD–16°4826	HDE 229232
P (d)	6.340±0.004	13.8194±0.0003	13.4±0.6	15.8±1.3	6.2±0.2
T_0 (HJD – 2,400,000.0)	53033.69±0.08	31212.0±0.2	53158.6±0.8	53162.8±1.8	54790.6±0.1
γ (km s ⁻¹)	8.5±1.1	-40.1±0.7	-4.9±1.1	11.0±1.0	-46.6±0.8
K_1 (km s ⁻¹)	22.2±1.5	13.1±1.0	26.2±1.5	13.1±1.6	15.6±1.2
$f(m)$ (M_\odot)	0.007±0.001	0.0032±0.0007	0.025±0.005	0.004±0.002	0.002±0.001
$a_1 \sin i$ (R_\odot)	2.8±0.2	3.6±0.3	6.9±0.5	4.1±0.6	1.9±0.2
rms (km s ⁻¹)	6.1	5.7	6.1	3.2	7.3
N	33	31	16	11	7

Table 3. Individual Stellar Parameters

Object Name	Spectral Classification	T_{eff} (kK)	$\log g$ (cm s ⁻²)	$v \sin i$ (km s ⁻¹)	Spectral Classification from ($T_{\text{eff}}, \log g$)	M_V (mag)	$E(B - V)$ (mag)	Distance (kpc)
(1)	(2)	(3)	(4)	(5)	(6)	(7)	(8)	(9)
HDE 308813	O9.5 V	29.9±0.3	3.73±0.09	204±10	B0 V ^a	-3.90	0.30	2.82
HD 152147	O9.7 Ib	27.8±0.5	3.10±0.06	150±28	O9.5 I ^a	-6.28	0.61	2.11
HD 164536	O9 III	37.4±0.9	4.25±0.17	230±14	O6.5 V ^b	-4.77	0.22	1.78
BD–16°4826	O5	39.9±6.3	4.04±0.40	131±28	O5.5 V ^b	-5.07	1.24	1.60
HDE 229232	O4 Vn((f))	41.7±1.3	4.05±0.14	273±19	O5 V ^b	-5.21	1.12	1.79

^aCalibration of Böhm-Vitense (1981).

^bCalibration of Martins et al. (2005).

Note. — Spectral classification references: HDE 308813: Schild (1970); HD 152147: Walborn (1972); HD 164536: MacConnell & Bidelman (1976); BD–16°4826: Hiltner & Johnson (1956); HDE 229232: Walborn (1973).

Table 4. Probable Unseen Companion Parameters

System (1)	$f(m)$ (M_\odot) (2)	M_1 (M_\odot) (3)	q (4)	M_2 (M_\odot) (5)	Estimated Secondary Spectral Classification (6)	ΔV (mag) (7)	Flux Ratio (f_2/f_1) (8)	$\frac{K_1(1+1/q)}{v \sin i}$ (9)	$v \sin i$ (sync) (km s $^{-1}$) (10)
HDE 308813	0.007	14	0.26	3.4	B7 V	2.7	0.08	0.53	20
HD 152147	0.003	28	0.18	5.0	B4 V	4.8	0.01	0.55	23
HD 164536	0.025	28	0.30	8.3	B2 V	2.3	0.12	0.49	13
BD–16°4826	0.004	34	0.19	6.4	B3 V	3.1	0.06	0.67	9
HDE 229232	0.002	38	0.16	5.9	B3 V	3.2	0.05	0.45	29

Table 5. Mass Ratios and Inclinations for Various Mass Ratio Distributions

System	q			$i(^{\circ})$		
	$\alpha = -1.35$	$\alpha = 0.0$	$\alpha = 1.0$	$\alpha = -1.35$	$\alpha = 0.0$	$\alpha = 1.0$
HDE 308813	0.15	0.26	0.43	35.5	20.5	6.0
HD 152147	0.10	0.19	0.38	30.4	16.6	10.5
HD 164536	0.18	0.30	0.45	37.0	22.7	12.6
BD–16°4826	0.11	0.19	0.39	32.4	18.3	13.1
HDE 229232	0.09	0.16	0.36	28.0	15.4	7.4

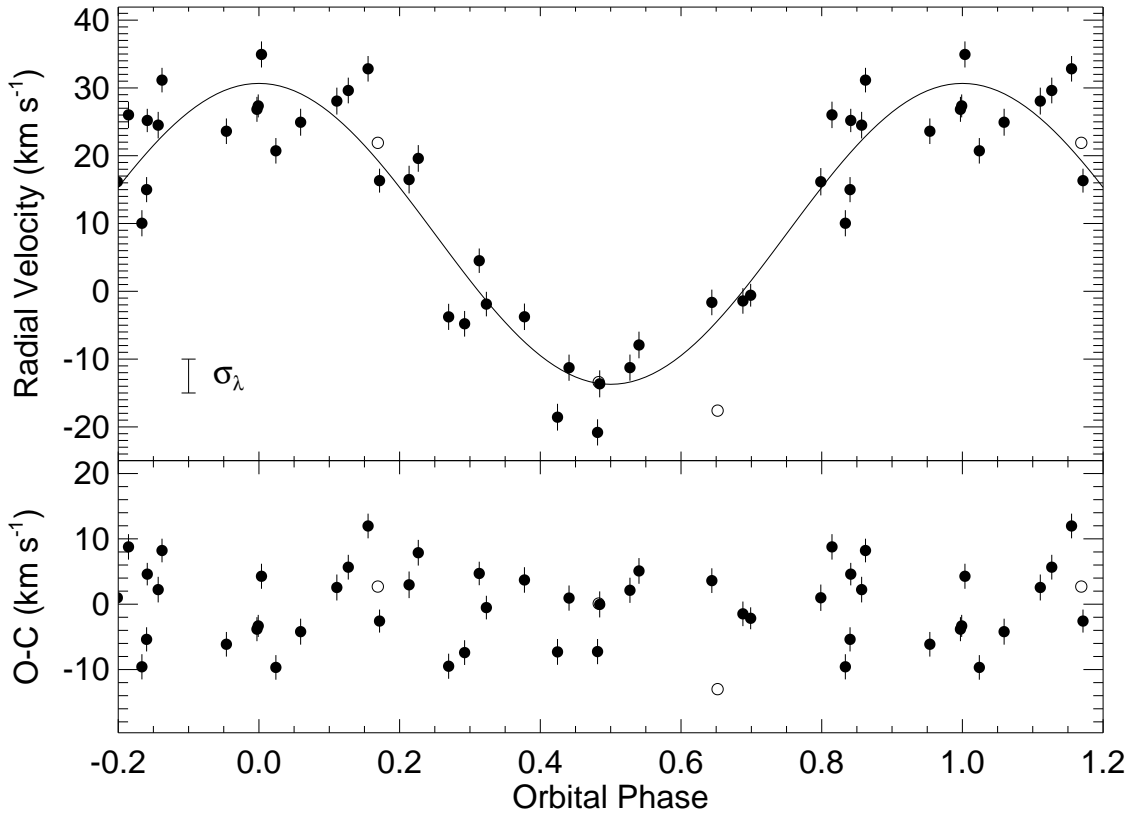


Fig. 1.— Radial velocities for HDE 308813. Filled circles are data from this analysis with uncertainties shown by line segments, and open circles are data from Huang & Gies (2006). Plotted beneath the velocities are the observed minus calculated values based on the circular orbital fit. Also shown is the 5 km s^{-1} uncertainty associated with the wavelength calibration.

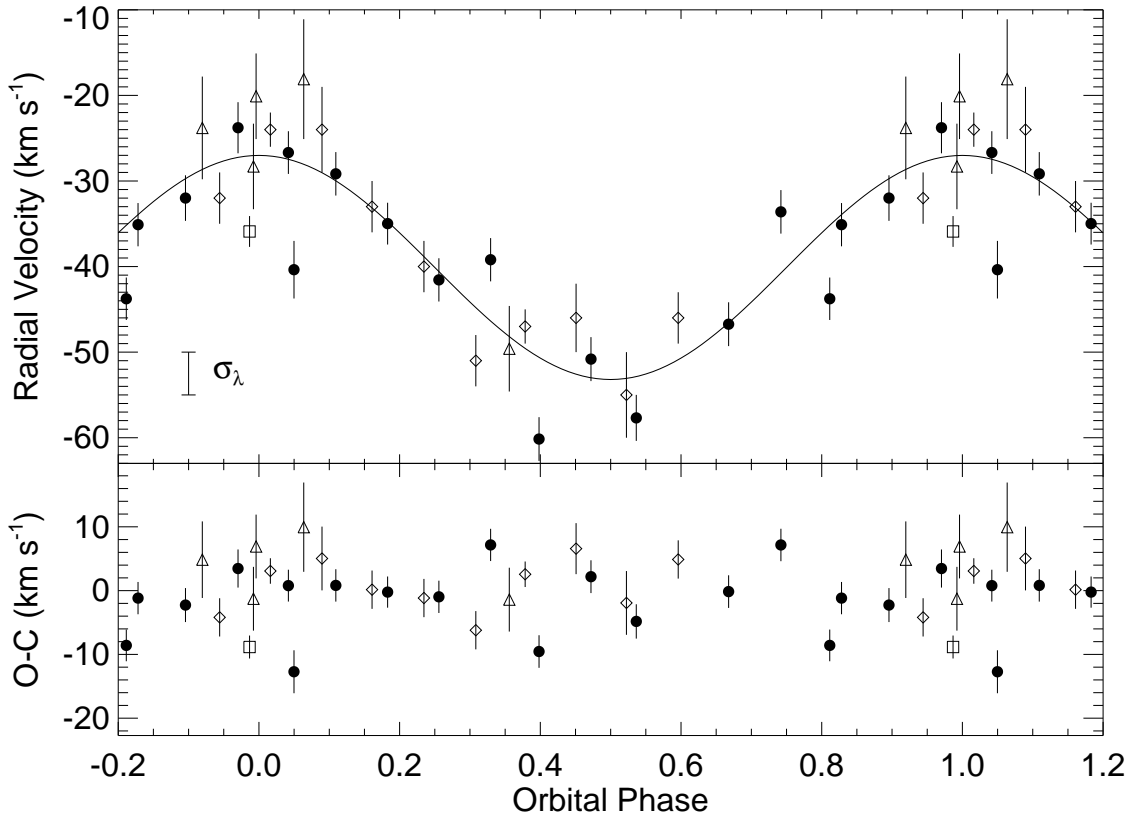


Fig. 2.— Radial velocities for HD 152147. Filled circles are data from this analysis, the open square is from Conti & Ebbets (1977), open triangles are from Struve (1944), and open diamonds are from Levato et al. (1988), with uncertainties shown by line segments. Plotted beneath the velocities are the observed minus calculated values based on the circular orbital fit.

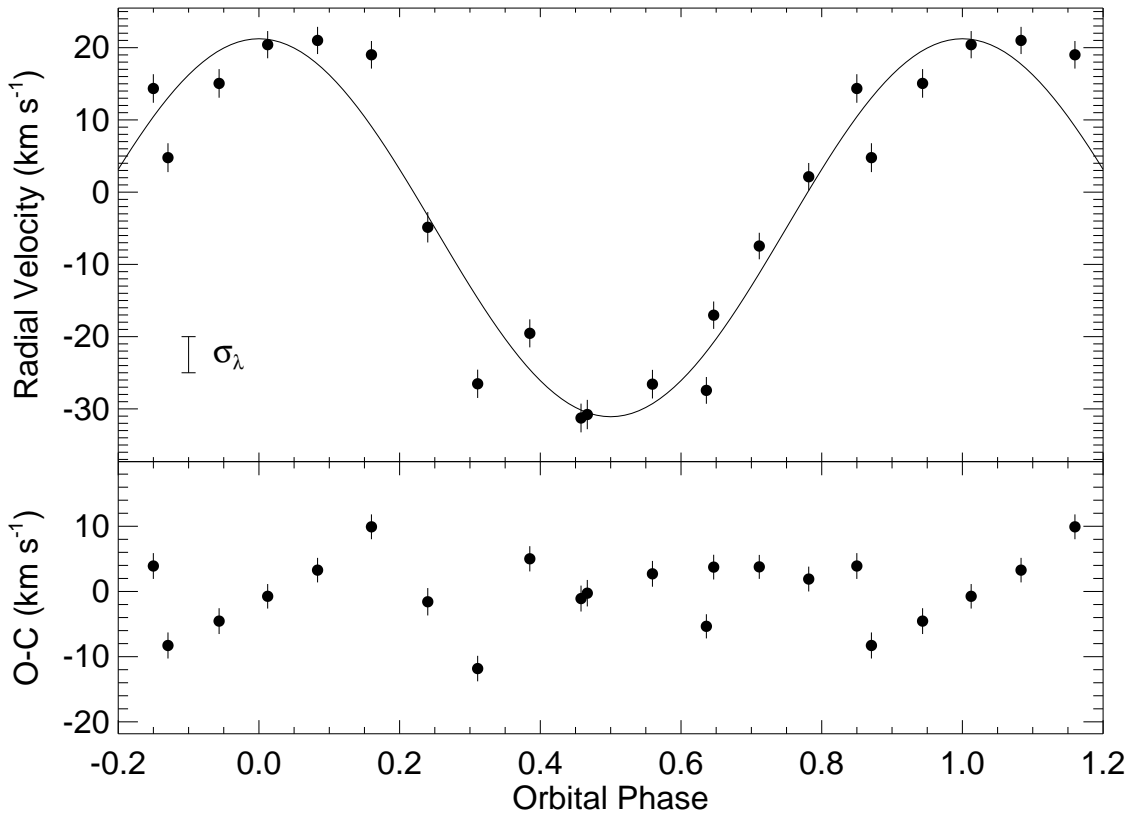


Fig. 3.— Radial velocities for HD 164536. Filled circles are data from this analysis, with uncertainties shown as line segments. Plotted beneath the velocities are the observed minus calculated values based on the circular orbital fit.

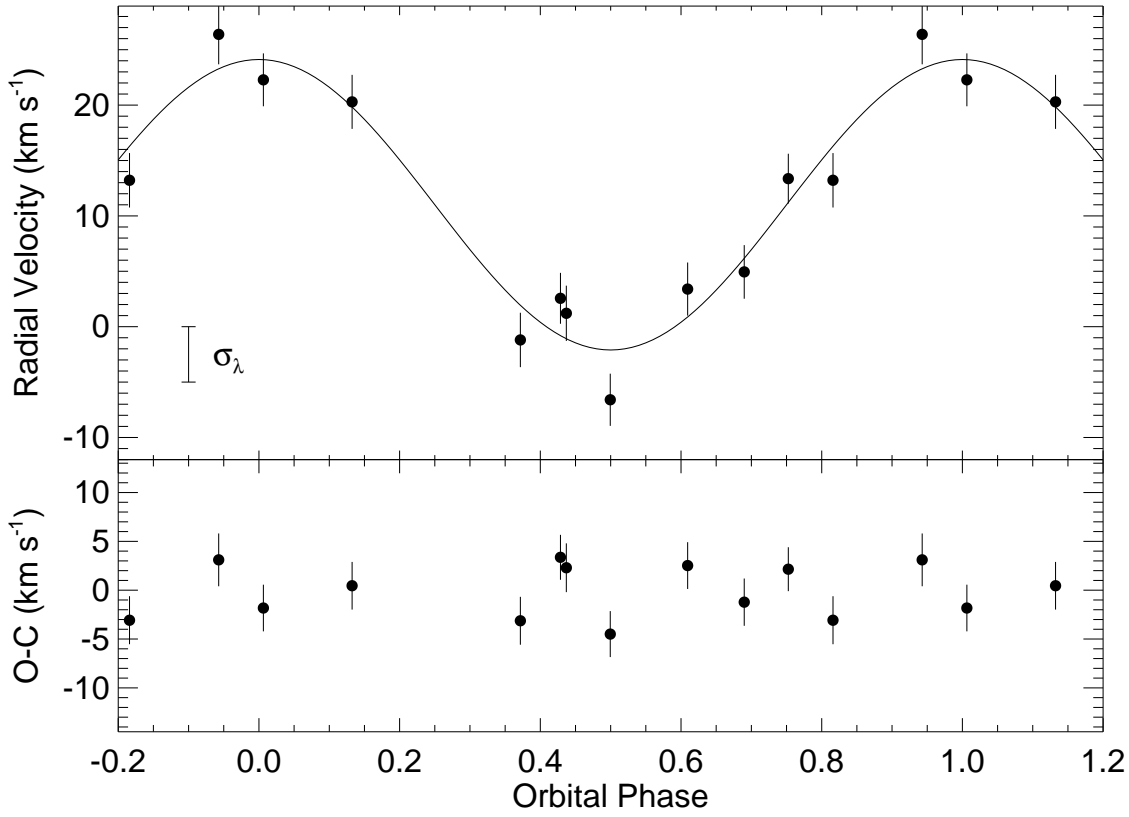


Fig. 4.— Radial velocities for BD–16°4826. Filled circles are data analyzed here, with uncertainties shown as line segments. Plotted beneath the velocities are the observed minus calculated values based on the circular orbital fit.

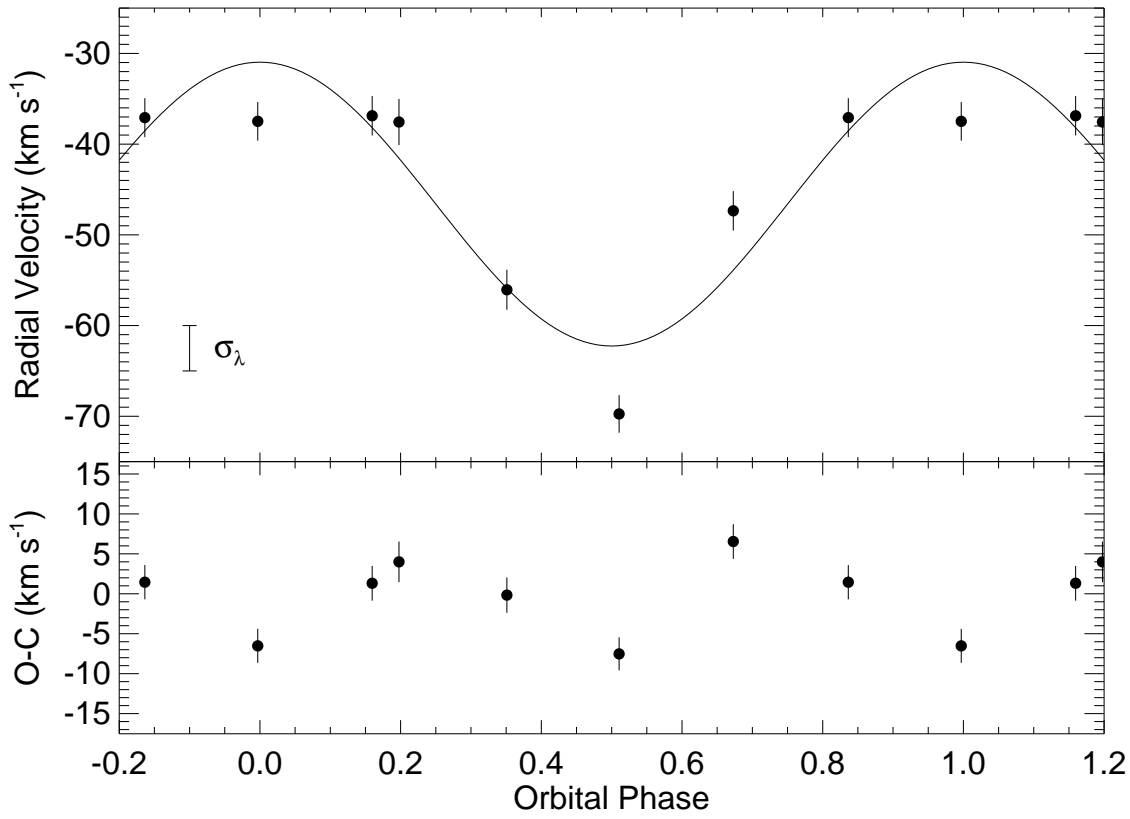


Fig. 5.— Radial velocities for HDE 229232. Filled circles are data from this analysis, with uncertainties shown as line segments. Plotted beneath the velocities are the observed minus calculated values based on the circular orbital fit.

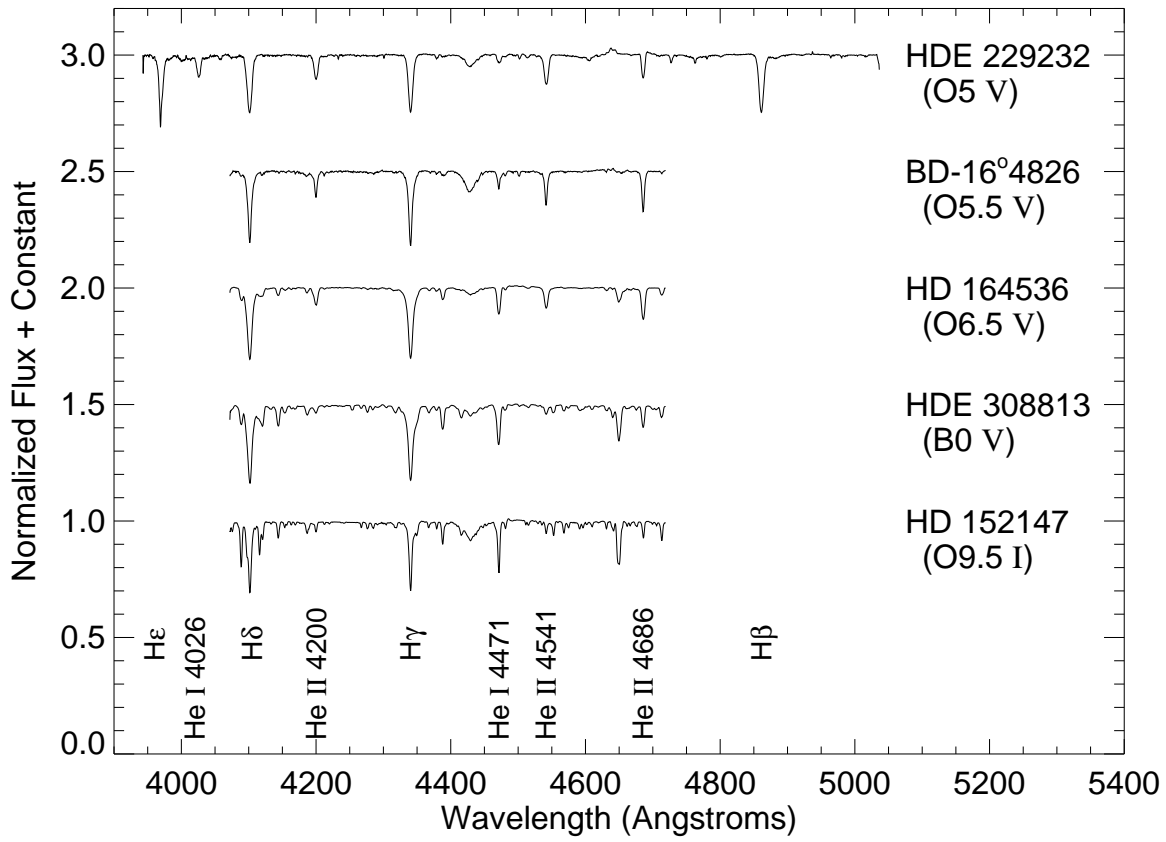


Fig. 6.— Spectra and prominent spectral features for objects discussed here. The hottest star is at top and targets are then plotted in order of decreasing effective temperature.